PHYSICAL REVIEW B VOLUME 35, NUMBER 9 15 MARCH 1987-II

Defect clusters in wustite $Fe_{1-x}O$

M. R. Press and D. E. Ellis
Department of Physics and Astronomy, and Materials Research Center, Northwestern University, Evanston, Illinois 60201
(Received 2 October 1986)

The electronic structure and stabilization energy of isolated defects and defect clusters in wustite $Fe_{1-x}O$ is studied by the first-principles local-density theory. The embedded-cluster model is used to obtain linear combination of atomic orbitals expansions of one-electron properties in the discrete-variational scheme. The stability of the 4:1 interstitial cluster relative to simple defects is verified, and the tendency of 4:1 clusters to aggregate is explored. Open edge- and vertex-shared aggregates which permit the close approach of charge-compensating Fe^{3+} ions are found to be energetically favored.

I. INTRODUCTION

There are three known oxides of iron, with ideal compositions FeO (wustite), Fe_2O_3 (hematite), and Fe_3O_4 (magnetite). The lowest oxide, wustite, exists as a stable phase only above 570 °C and has a rock-salt structure. Cumulative over the past two decades, starting with the seminal work of Roth,[1] diffraction studies have shown that wustite has a cation-deficient nonstoichiometric structure $Fe_{1-x}O$ ($0.05 < x < 0.15$); this involves not just x iron vacancies with $2x$ ferrous ions oxidized to the ferric state, but also defect clusters in which some ferric ions occupy interstitial tetrahedral sites. The x-ray diffraction work of Koch and Cohen[2] on quenched single crystals clearly indicates a superlattice-generating cluster which is cubic, and the presence of vacancies in nearest-neighbor cation sites surrounding tetrahedral ions. Furthermore, neutron diffraction intensity ratios as calculated by Cheetham *et al.*[3] allow the determination of the ratio of the number of octahedral vacancies (m) to the number of tetrahedral interstitials (n), $r = m/n$, which is now accepted to be 2.5–3.0 for wustite. r is believed to increase with temperature and at lower defect concentrations, a fact which suggests the dissociation of larger vacancy aggregates into smaller "basic" clusters built from an interstitial ferric ion surrounded by 4 cation vacancies, namely, the 4:1 (m:n) cluster shown in Fig. 1. Lattice relaxations in the form of static and dynamic displacements ~ 0.2 Å of ions surrounding a defect are also detected. Diffraction data[4] has also been interpreted in terms of an ordered defect phase having commensurate cubic superstructure based on idealized wustite with lattice constant $5a$. Catlow and Fender[5] have employed lattice-energy calculations based on the Born model to identity the 4:1 cluster as the basic cluster and tend to believe that stable small edge-sharing aggregates of the 4:1 defect (e.g., a 6:2 or 8:3 defect) give way energetically to more extended corner-sharing aggregates (e.g., a 16:5 spinel-like structure). More recently, a quantum mechanical approach by Anderson *et al.*[6] using predominantly covalent normalized ion energies yielded 13:5 and 16:7 defect clusters as having the proper structure and composition to account for the observed phases in wustite.

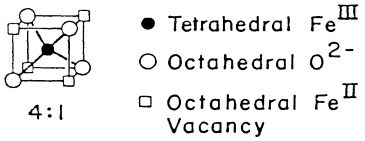

FIG. 1. Schematic of the 4:1 defect cluster.

In the present effort, we have carried out a study of *ab initio* binding energies of possible defect clusters in $Fe_{1-x}O$, wherein we have attempted to answer questions such as the following: (a) Is there a simplest or basic stable defect in $Fe_{1-x}O$, and (b) if so, what is the mode of aggregation of this basic defect to form larger defects? We employ the embedded- molecular-cluster model within the framework of the Hartree-Fock-Slater (HFS) self-consistent one-electron local-density theory[7] using the discrete-variational (DV) method with a linear combination of atomic orbital-molecular orbital (LCAO-MO) basis to obtain the electronic structure, charge densities, density of states, and potentials for the defects studied. We then set up an algorithm for the calculation of the cohesive energy in periodic solids and the internal energy of formation of the prototypical defects studied. These defects include a cation vacancy, an octahedral ferric cation, the series of simple defects 1:0, 2:0, 0:1, 1:1, 2:1, 3:1, 4:1, and the series 6:2, 8:3, 7:2 ⟨110⟩, 7:2 ⟨111⟩, 8:2, and 13:4. Our aim is not so much to obtain the exact defect structure that maximizes the binding, but rather to study the mechanisms of growth and the competing energy trends in the formation of simple and aggregate defects.

For some time now, the DV-HFS method has proved itself capable of calculating the binding energy of molecules and small clusters of atoms to desired precision. For instance, Delley *et al.*[8] have investigated the equilibrium geometry, binding energy, and electronic structure of small Cu clusters; Guo and Ellis[9] have carried out self-consistent cluster calculations for the binding energy of positive muons in Cu. Our work then represents a natural extension to the study of bulk solids, both perfect or with periodicity-destroying vacancies, impurities, and distortions. Any embedding scheme used to join molecular

clusters to the host medium raises a number of points beyond those considered for a free cluster. They involve the choice and implementation of physically reasonable embedding conditions and the construction of a model Hamiltonian containing cluster-host and intracluster Coulomb and exchange-correlation interactions. In total- and binding-energy calculations, further questions need to be answered; for instance, to what zero of energy does one reference the eigenvalues and potential? How does one ensure a minimum energy configuration for a defect cluster? Since the defect clusters come in varied shapes and sizes and are embedded in a crystal potential that itself changes in response to the defects, is it legitimate to incorporate results from one cluster calculation in another?

II. THEORETICAL-COMPUTATIONAL PROCEDURE

In the LCAO-MO method applied to solids,[10] the wave functions and eigenvalues of a cluster of atoms extracted from the solid are calculated; the rest of the solid manifests its presence by providing an electrostatic crystal field and charge field in which the cluster is embedded. The essential idea is to suppress surface or cluster-size effects by making the peripheral atoms sense a potential similar to that found in the bulk crystal. This is known to accelerate the convergence of such properties as the charge distribution and the density of states; not so other properties such as the magnetization that appear to depend critically on wave-function localization which is severely restricted in small clusters. This method has proved to be very conducive to the study of systems with low symmetry or with defects for which the conventional band-structure approach proves intractable or computationally expensive. The potential field is simulated by constructing a microcrystal surrounding the cluster consisting of all atoms placed at their equilibrium lattice positions (or in predetermined or desired positions when studying defects), and employing a self-consistency procedure to generate a Coulomb and exchange-correlation potential field in which the cluster is immersed. Typically, the microcrystal extends out to 17—20 a.u. from the center of the cluster and includes about 250—300 of the surrounding atoms.

The nonrelativistic one-electron Hamiltonian in the HFS model[7–11] of the self-consistent one-electron local-density (LD) formalism can be written in Hartree atomic units as

$$H(\mathbf{r})=-\tfrac{1}{2}\nabla^2+\int\frac{\rho(\mathbf{r}')}{|\mathbf{r}-\mathbf{r}'|}d\mathbf{r}'-\sum_\nu\frac{Z_\nu}{|\mathbf{r}-\mathbf{R}_\nu|}+V_{\mathrm{xc},\sigma}(\mathbf{r})\ . \tag{1}$$

The sum of the second and third terms, the electronic and nuclear contributions, constitute the Coulomb potential $V_C(\mathbf{r})$, while the truly nonlocal Hartree-Fock (HF) exchange-correlation operator $V_{\mathrm{xc},\sigma}$ for spin σ is approximated by the so-called $X\alpha$ potential dependent only on the local electron density,

$$V_{\mathrm{xc},\sigma}(\mathbf{r})=-\frac{3\alpha}{\pi}\left[\frac{3\pi^2}{4}\rho_\sigma(\mathbf{r})\right]^{1/3},\ \tfrac{2}{3}\le\alpha\le 1\ . \tag{2}$$

Molecular-orbital eigenfunctions $\psi^\beta_{i\sigma}(\mathbf{r})$ to the above one-electron Hamiltonian are most conveniently expanded in terms of a basis set of symmetry orbitals $\{\phi^\beta_j(\mathbf{r})\}$,

$$\psi^\beta_{i\sigma}(\mathbf{r})=\sum_j\phi^\beta_j(\mathbf{r})C^\beta_{ji\sigma},\ \beta=(k\lambda)\ . \tag{3}$$

$\phi^\beta_j(\mathbf{r})$ are chosen to be those LCAO-MO centered on the different cluster atom sites that transform as the λth row of the kth irreducible representation of the cluster point group, i.e.,

$$\phi^\beta_j(\mathbf{r})=\sum_\nu\sum_m R_{nl}(r_\nu)Y_{lm}(\hat{\mathbf{r}}_\nu)e^{\nu j}_{lm} \tag{4}$$

with $r_\nu=|\mathbf{r}-\mathbf{r}_\nu|$. Here radial wave functions $R_{nl}(r_\nu)$ constitute a free atom or ion basis set with principal quantum number n and orbital quantum number l and the coefficients $e^{\nu j}_{lm}$ can be calculated by group theoretical means.[12] Then the standard condition that the expectation value of the operator $(H-\varepsilon)$ be stationary with respect to variations in $C^\beta_{ji\sigma}$ leads to a set of Rayleigh-Ritz type secular equations compactly written in matrix form as

$$(H-\varepsilon S)C=0\ . \tag{5}$$

In the discrete-variational method (DVM),[13] the Hamiltonian matrix H and the orbital-overlap matrix S are evaluated as weighted sums over a set of sampling points $\mathbf{r}_k$ with weight function $W(\mathbf{r}_k)$, i.e.,

$$H_{ij}=\sum_R W(\mathbf{r}_k)\phi^{\beta*}_i(\mathbf{r}_k)H\phi^\beta_j(\mathbf{r}_k) \tag{6a}$$

and

$$S_{ij}=\sum_R W(\mathbf{r}_k)\phi^{\beta*}_i(\mathbf{r}_k)\phi^\beta_j(\mathbf{r}_k)\ . \tag{6b}$$

The sampling point set consists of an optimized Gaussian surface mesh[14] in conjunction with a Gauss-quadrature radial grid[15] for the core region around each nucleus and a diophantine distribution[13] in the interstitial region beyond the spheres. By choosing the diophantine weight function to be simply the local volume per point, i.e., the inverse of the sampling point density, we cause our weighted sums to converge towards Rayleigh-Ritz matrix elements in the limit of an infinite number of points.

Solving secular Eq. (5) for the coefficients C^β_{ji} yields molecular-orbital (MO) eigenfunctions $\psi^\beta_i(\mathbf{r})$ and their eigenvalues ε_i. The lowest-energy MO's are filled successively with the cluster electrons up to a self-consistently determined Fermi energy using Fermi-Dirac statistics. The cluster charge density on the variational grid is obtained by summing over all N MO's,

$$\rho^{\mathrm{cluster}}_\sigma(\mathbf{r})=\sum_{i=1}^N f_{i\sigma}\,|\,\psi_{i\sigma}(\mathbf{r})\,|^2\ , \tag{7}$$

where $f_{i\sigma}$ are the Fermi-Dirac occupation numbers. In the so-called self-consistent-charge (SCC) approximation, the charge density is projected onto the multicenter atomic radial functions,

$$\rho^{\mathrm{cluster}}_\sigma(\mathbf{r})\cong\rho^{\mathrm{SCC}}_\sigma(\mathbf{r})=\sum_\nu\sum_{n,l}A^\nu_{nl}\,|\,R_{nl}(r_\nu)\,|^2\ . \tag{8}$$

The occupation numbers A_{nl}^{ν} for the atomic orbitals are obtained by a diagonal-weighted Mulliken population analysis of the charge density;[16] alternately a least-squares fitting to $\rho_{\sigma}^{\text{cluster}}$ is also possible. This yields the total charge density

$$\rho^{\text{tot}}(\mathbf{r})=\rho^{\text{cluster}}(\mathbf{r})+\rho^{\text{ext}}(\mathbf{r}) . \tag{9}$$

The Coulomb potential from each spherically symmetric charge distribution is given by the one-dimensional integral

$$V_c^i(r)=4\pi\left[\frac{1}{r}\int_0^r \rho(r')r'^2dr' + \int_r^{\infty}\frac{\rho_i(r')}{r'}r'^2dr'\right]-\frac{Z_i}{r} . \tag{10}$$

The total nonspherical Coulomb potential is simply the sum of all the spherically symmetric contributions from all the atoms in the microcrystal, rewritten by means of a generalized Ewald-type summation,[17] using Gaussian charge distributions around the nuclei, as a sum of two rapidly convergent series,

$$V_c^{ew}(\mathbf{r})=\left[\frac{4\pi}{\Omega_0}\sum_{\mu}{}'\sum_i Q_i\frac{e^{-k_\mu^2/4g^2}}{k_\mu^2}\cos[\mathbf{k}_\mu\cdot(\mathbf{r}-\tau_{il})]\right] + \sum_i\left[V_c^i(r_i)-Q_i\frac{\text{erf}(r_i g)}{r_i}\right] . \tag{11}$$

Here τ_{il} is the coordinate of the ith atom in unit cell l, carrying net charge Q_i; g is the half-width of the Gaussian, properly chosen to ensure rapid convergence of both components and the $\mathbf{k}$-vector sum over μ extends out to a $\mathbf{k}_{\max}$ determined by the precision to which the potential is required. The first term in Eq. (11) which arises from a smoothed-out charge distribution is considered a property of the undistorted lattice and is left intact. Then by manipulating the neutralizing Gaussian charges piled around the point nuclei, the presence of defects of any kind can be treated simply as a correction to the second short-range term in Eq. (11). This makes it possible for us to introduce "virtual" atoms (essentially unoccupied basis orbitals) at vacancy positions which provide for additional variational freedom without much addition to computation time. Finally, electrons in the cluster sampling the potential wells of atoms external to the cluster tend to lower the energy of the valence orbitals as they try to occupy these wells. In reality, the cluster wave functions must remain orthogonal to the occupied exterior atom states. This repulsive effect is simulated in a simple manner by truncating the deep potential wells around the external atom nuclei at some radius R_w to some value V_w typically chosen at about the Fermi energy.

The standard expression for the total energy in the local-spin-density approximation[18,8] is the following:

$$E_t=\sum_{\sigma}\left[\sum_i f_{i\sigma}\varepsilon_{i\sigma}-\tfrac{1}{2}\int\int\frac{\rho_\sigma(\mathbf{r})\rho(\mathbf{r}')}{|\mathbf{r}-\mathbf{r}'|}d\mathbf{r}\,d\mathbf{r}' + \int\rho_\sigma(\mathbf{r})\left[E_{\text{xc},\sigma}(\mathbf{r})-V_{\text{xc},\sigma}(\mathbf{r})\right]d\mathbf{r}\right] + \tfrac{1}{2}\sum_{\mu}\sum_{\nu}{}'\frac{Z_\mu Z_\nu}{r_{\mu\nu}} \tag{12}$$

where the exchange-correlation energy $E_{\text{xc},\sigma}(\mathbf{r})$ and the exchange-correlation contribution to the chemical potential $V_{\text{xc},\sigma}(r)$ are related by

$$E_{\text{xc},\sigma}(\mathbf{r})=\tfrac{3}{4}V_{\text{xc},\sigma}(\mathbf{r})$$

for the Kohn-Sham potential. In a free cluster, the integrals are evaluated by discrete summation of points extending over all space. In a solid system, the integrals need to be computed over a suitably chosen representative volume Ω_0, perhaps corresponding to a unit cell or a molecular formula unit. Since the cluster need not have the same stoichiometry as the crystal, the eigenvalue sum is rewritten as $\int\rho_\varepsilon(\mathbf{r})\,d\mathbf{r}$, where

$$\rho_\varepsilon(\mathbf{r})=\sum_{i,\sigma}f_{i\sigma}\varepsilon_{i\sigma}|\psi_{i\sigma}(\mathbf{r})|^2$$

is a local "eigenvalue density" at point $\mathbf{r}$, and also defines a local kinetic-energy density and a local energy density at point $\mathbf{r}$.

Total energies calculated in this fashion typically are of the order of 10^5 eV, and with the sampling schemes chosen are not calculated accurately enough for direct comparison of energy differences. However, it is possible to extract a much more accurate binding energy with respect to some reference system, say, the dissociated solid,

$$E_g=E_t^{\text{sys}}-E_t^{\text{ref}} . \tag{13}$$

The reference state of the separated atoms must be treated by spin-unrestricted density-functional formalism since spin-dependent exchange energy is an important contribution in isolated-atom energies. It has been shown[8] that for a choice of a linear sampling operator, both $E_t[\rho]$ and $E_t^{\text{ref}}[\rho]$ are stationary with respect to the density ρ and the variational basis $\{\phi_i^\beta\}$. So numerical noise is minimized by computing the reference system energy over the same volume with the same sampling grid with the atoms in the same position but now assumed to be noninteracting. Thus cohesive energy values, of the order of a few electron volts, are converged to better than 0.01 eV. In considering a defect structure in a crystal, there is no particular volume Ω_0 corresponding to the defect cluster over which to evaluate the discrete-integral terms in Eq. (13). These integrals are now computed over all unit cells for which the contributions to the binding energy of the defect structure crystal differ from the contribution to the binding energy of the idealized crystal. For the largest defect clusters treated here, this involves all primitive cells within about $2.5a$ from the cluster origin.

Typically, the total energy of atoms calculated via the statistical total-energy functional $E_t[\rho]$, using the Kohn-

Sham local exchange potentials differs by about 1% from the HF result, which is a strict upper bound to the total energy. Further, the absolute error in total energy is a rapidly increasing function of the atomic number. This is due mostly to large errors in the deepest-lying core states and is traced to the inaccurate treatment of the self-interaction part of the exchange operator. Since we are interested here in comparison of systems whose core states are barely changed, this aspect of the problem is unimportant for valence electron derived properties and explains why the accuracy of our computed cohesive energies greatly exceeds the absolute accuracy of either the atomic or the solid calculations. Lastly, for charged clusters, it is useful to partition the sum of single-particle eigenvalues into its contributions from the different atoms ν in the cluster by

$$\int \rho_\varepsilon(\mathbf{r})\,d\mathbf{r} = \int \sum_\nu \rho_\varepsilon^\nu(\mathbf{r})\,d\mathbf{r}\ , \tag{14}$$

where $\rho_\varepsilon^\nu(\mathbf{r})$ is obtained from a diagonal-weighted Mulliken analysis of ρ_ε. Using this and Eqs. (12) and (13), we can calculate the cohesion of a single atom or ion in the crystal environment as well as average binding energies per molecular unit.

Finally, comparison between theoretical results and spectroscopic data is made possible by calculating the local density of states (LDOS)

$$d_{nl}^\nu(\varepsilon) = \sum_p f_{nl,p}^\nu \frac{\gamma/\pi}{(\varepsilon-\varepsilon_p)^2+\gamma^2} \tag{15}$$

and the total density of states (DOS),

$$D(\varepsilon) = \sum_{\nu,n,l} d_{nl}^\nu = \sum_p \frac{\gamma g_p/\pi}{(\varepsilon-\varepsilon_p)^2+\gamma^2}\ , \tag{16}$$

where $f_{nl,p}^\nu$ is the population contribution from atom ν, state (n,l) to the pth molecular orbital and g_p is the degeneracy of level ε_p. The Lorentzian width parameter γ, chosen to be about 0.40 eV, provides the smoothing out of the discrete level structure to simulate solid-state bands.

The formation of a defect cluster by removing Fe atoms from a stoichiometric wustite lattice is best represented as

$$\begin{aligned} 3(m-n)\mathrm{Fe}^{++}(\mathrm{O}) \rightarrow\ & n\mathrm{Fe}^{+++}(t) + mV_{\mathrm{Fe}} \\ & + (2m-3n)\mathrm{Fe}^{+++}(\mathrm{O}) \\ & + (m-n)\mathrm{Fe}^{0}(\infty)\ , \end{aligned} \tag{17}$$

i.e., the presence of n-trivalent Fe ions in tetrahedral (t) sites is accompanied by the creation of m cation vacancies screened by $2m-3n$ octahedral (O) ferric ions and the expulsion of $m-n$ Fe atoms. For example, in the case of the 4:1 cluster, the equation would read

$$9\mathrm{Fe}^{++}(\mathrm{O}) \rightarrow 1\mathrm{Fe}^{+++}(t) + 4V_{\mathrm{Fe}} + 5\mathrm{Fe}^{+++}(\mathrm{O}) + 3\mathrm{Fe}^{0}(\infty)\ . \tag{18}$$

We have chosen to write the ionic charges as $(++)$ or $(+++)$ instead of $(+2)$ or $(+3)$ to indicate self-consistently determined spin and orbital occupation numbers and ionicities rather than the nominally predicted chemical ionicities. Equation (18) is strictly balanced for charge, mass, and sites, an essential feature since the minimum energy structure is one where the microcrystal has zero overall charge.

In the integration scheme, roughly 600 points per atom are used, split between a 30×12 (radial$\times$angular) Gauss-quadrature grid out to 1.5 a.u. and diophantine points beyond in the interstitial regions. However, for the large 27 atom clusters this number is reduced to 450 points per atom (with a 24×12 G-q grid), a step forced by the need to keep computing space and time within manageable limits. Ionic basis sets for $\mathrm{Fe}(+2)$, $\mathrm{Fe}(+3)$, and $\mathrm{O}(-2)$, compacted by a smooth potential well of depth 2.0 a.u. out to 6.0 a.u., are chosen. Orbitals $3d$, $4s$, $4p$ for Fe and $2s$, $2p$ for O were chosen to provide a modest degree of variational freedom. The lower-lying orbitals for each atom form a part of the frozen or nonvariational core. The contribution of the shift in core eigenvalues to the one-electron eigenvalue sum is given to a good first approximation by $\int \rho_0^c(\mathbf{r})\Delta V(\mathbf{r})d\mathbf{r}$, where $\rho_0^c(\mathbf{r})$ is the core charge density at $\mathbf{r}$ and $\Delta V(\mathbf{r})$ is the change in potential at $\mathbf{r}$ in going from a free atom to a solid. Vacancy sites are provided with unoccupied $1s$ and $2p$ virtual orbitals, compacted with the same potential well as above. The microcrystal extends outwards, spherically or cylindrically depending on the shape of the cluster, to include about 250—300 of the closest atoms and the pseudopotential cutoff is fixed at 0.0 a.u. (relative to E_F) out to a radius of 1.8 a.u. about each exterior crystal atom. The scaling factor in the $X\alpha$ exchange potential is chosen to be $\alpha=0.70$ in all our calculations, a value near the classical Kohn-Sham derivation, and found to be nearly optimal in molecular studies.

III. RESULTS AND DISCUSSION

A. Idealized wustite FeO

A spin-polarized numerical calculation with $\alpha=0.70$ on the free Fe atom $(3d^6,4s^2)$ gives the total energy as -1261.57 a.u. (1 a.u.$=27.211\,65$ eV). The corresponding numerical HF result is -1262.291 a.u., i.e., the local density approximation is subject to relative errors in total energy of transition metals of the order of 10^{-3}. A similar total-energy calculation for atomic O $(2s^2,2p^4)$ yields -74.3565 a.u.; the HF result is -74.80936 a.u. We note that in the original $X\alpha$ scheme one would adjust α to make the HF and LD energies equal. However, this approach leads to different α values in different crystalline regions and constitutes a poorly controlled approximation for our purposes.

Given the rocksalt structure of a stoichiometric FeO lattice, two very obvious choices to study its structural properties are a neutral embedded 8-atom cluster Fe_4O_4 and a dense-packed 27-atom cluster $Fe_1O_6Fe_{12}O_8$, that includes all the atoms in the cubic unit cell. In Fig. 2 the cohesive energy of FeO as calculated from the former is plotted and its properties are tabulated in row 1 of Table I. The lattice constant obtained is 8.21 a.u. which is within 0.8% of the experimental value of 8.15 a.u. quoted in Wyckoff.[19] The cohesive energy is calculated to be 11.20 eV with respect to free atoms; the experimental

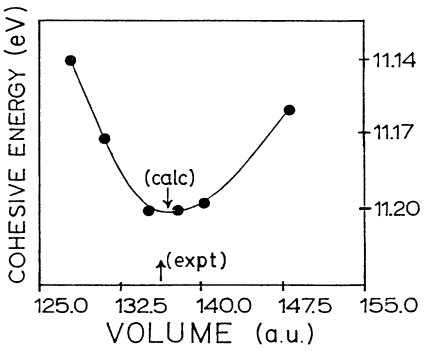

FIG. 2. Cohesive energy in idealized FeO versus lattice volume parameter.

value is 40.17 eV (Ref. 20) with respect to isolated gaseous ions, or equivalently (40.17−24.08+6.57) eV=22.66 eV with respect to isolated gaseous atoms after using the second ionization potential for Fe and the electron affinity for O. The smallness of our cohesive energy is clearly a consequence of the very restricted basis set we use. A diagonal-weighted Mulliken population analysis of the charge density gives orbital occupation numbers and spin for Fe($3d^{5.85}$, $4s^{0.20}$, $4p^{0.05}$; spin, $4.34\mu_B$) and O($2s^{2.0}$, $2p^{5.90}$; spin, $0.11\mu_B$) that closely resemble the standard chemical values for free ions. The *d-s* gap, i.e., the energy difference from the top of the Fe $3d$ band to the next set of orbitals (Fe $4s$ and minority spin Fe $3d$) is 3.10 eV and the chosen form of the crystal pseudopotential stabilizes the Fermi level at −2.78 eV. The $4s$ levels are concentrated just above the Fermi energy, extending up to 2.0 eV.

Grenet *et al.*[21] have reported well-resolved x-ray photoemission spectra (XPS) and ultraviolet photoemission spectra (UPS) on a FeO single crystal showing 3 structures at 1.5, 4.3, and 7.8 eV which are deduced to be mainly Fe $3d$ in character and a single peak at 6.0 eV corresponding to $2p$ O. Other XPS measurements on wustite by Bagus *et al.*[22] show the Fe $3d$ valence-band states spread broadly over ~10 eV and an O $2p$ band located at 5.5 eV. The photoelectron spin-polarization (ESP) measurements by Alvarado, Erbudak, and Munz[23] yield a Fe $3d$ band centered about 4.2 eV and spread over ~7 eV

TABLE I. Study of defect-free FeO.

Cluster description	Cluster symmetry	No. valence electrons in cluster	No. cluster atoms	Fermi level (eV)	*d-s* gap (eV)	Self-consistent ionicities (spins)	Cohesive energy per ion pair (eV)
Fe_4O_4	T_d	56.0	8	−2.78	3.10	Fe_4 1.90 (4.34) O_4 −1.90 (0.11)	11.20
$Fe_2Fe_4O_2O_4$	D_{2h}	84.0	12	−2.67	2.42	Fe_2 1.93 (4.15) Fe_4 1.85 (4.34) O_2 −1.86 (0.10) O_4 −1.89 (0.08)	11.45
$Fe_4Fe_4O_4O_4$	D_{2d}	112.0	16	−2.34	2.41	Fe_4(in) 1.90 (4.15) Fe_4(out) 1.86 (4.35) O_4(in) −1.86 (0.09) O_4(out) −1.89 (0.07)	11.67
$Fe_1O_1Fe_4O_4Fe_2O_2$	C_{2v}	98.0	14	−2.61	1.87	Fe_1 1.97 (4.04) O_1 −1.80 (0.11) Fe_4 1.84 (4.31) O_4 −1.88 (0.06) Fe_2 1.91 (4.24) O_2 −1.89 (0.09)	11.24
$Fe_1Fe_6O_2O_6$	C_{3v}	105.9	15	−2.45	2.48	Fe_1 2.00 (4.07) Fe_6 1.88 (4.32) O_2 −1.90 (0.09) O_6 −1.89 (0.08)	10.96
$O_1O_6Fe_2Fe_6$	C_{3v}	104.1	15	−2.95	1.87	O_1 −1.68 (0.13) O_6 −1.88 (0.08) Fe_2 1.92 (4.29) Fe_6 1.83 (4.23)	10.80
$Fe_1O_6Fe_{12}O_8$	O_h	189.90	27	−2.04	2.25	Fe_1 1.87 (−4.02) O_6 −1.82 (0.11) Fe_{12} 1.87 (4.08) O_8 −1.92 (0.08)	11.31

and an O $2p$ band centered at 7 eV. In short, there are still points of dispute regarding the experimental data. All the energy values above are quoted with respect to the Fermi level. Typically, in $3d$ transition-metal oxides, the $3d$ metal electrons interact strongly with each other and with the surrounding anions to give rise to a set of localized states or narrow bands within the O $2p$-Fe $4s$ gap of about 6 eV. Conventional band-structure calculations, however, have had to be supplemented by semiempirical energy level schemes based on atomistic crystal-field theory (CFT) analysis in order to understand the positions and intensities of these spectral bands. Our DOS, shown in Fig. 3, displays a majority-spin Fe $3d$ valence band centered at -6.9 eV, an O $2p$ band at -10.2 eV, a small Fe $3d$ concentration admixed with $2p$ at -9.6 eV, and some O $2p$ density at -6.3 eV. Thus we have only two dominant peak structures, Fe $3d$ at 4.1 eV and O $2p$ at 7.4 eV relative to the Fermi energy. These results are directly attributable to the compressed nature of the ionic bases chosen for Fe and O, which leads to ionicities of ± 1.90 for Fe and O; the transfer of almost 2 electrons from Fe to O shows up in a ground-state calculation as an depletion of occupied DOS structure from the $3d$ levels and pushes the O $2p$ levels to lower energies. In Fig. 3, the discrete energy levels have been smoothed out to resemble bands by means of a 0.40-eV full-width-at-half-maximum Lorentzian function [Eqs. (15) and (16)]; thus the calculated widths of the d and p levels from the cluster atoms are uncertain by this amount. Further insight into the role of basis sets and reduced coordination numbers on the DOS is provided by the results of the 27-atom cluster.

The small size and symmetry of the 8-atom cluster—all cations treated identically—prevent us from investigating the antiferromagnetic nature of wustite (Néel temperature, 198 K). The 27-atom cluster $Fe_1O_6Fe_{12}O_8$ is distinctive in that it provides a central cation, fully coordinated to other cluster atoms, the direction of whose spin can be the subject of a detailed superlattice calculation, wherein the external crystal has alternate planes of cations with opposite spins, or a simpler calculation in which the external crystal potential is again generated via the results of the 8-atom cluster. Results from the latter calculation are shown in row 7 of Table I. The central Fe cation has a spin of -4.02, opposite in sign to the surrounding spins, while the other occupation numbers closely follow the 8-atom cluster results. The cohesive energy for this calculation is 11.31 eV; however, the energy difference between the two spin directions for the central cation is less than the precision to which the cohesive energy is calculated. For such a cluster with different sets of cations and anions in different environments, it is more instructive to look at the density of states from each inequivalent set, as shown in Fig. 4, rather than the cumulative DOS. Both the central Fe and the 12 peripheral Fe which are fourfold coordinated within the cluster exhibit a majority spin DOS structure centered at 4.0 eV. The anion set $\{O_8\}$ which is really equivalent to the anions in the Fe_4O_4 cluster provides a $2p$ contribution to the DOS located at 7.6

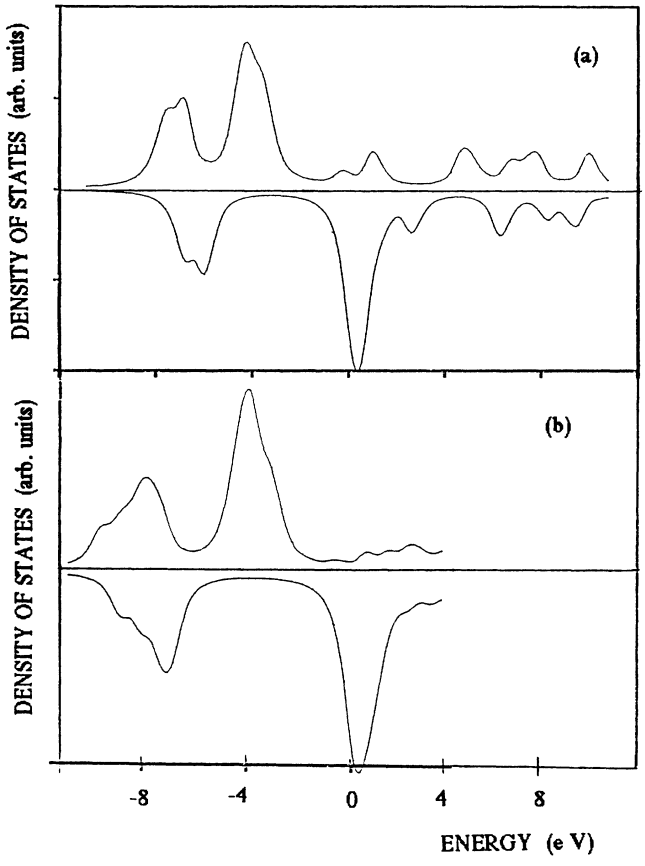

FIG. 3. Total densities of states in idealized FeO. Upper half panel is spin ↑; lower panel is spin ↓. (a) Fe_4O_4 cluster; (b) $FeO_6Fe_{12}O_8$ cluster.

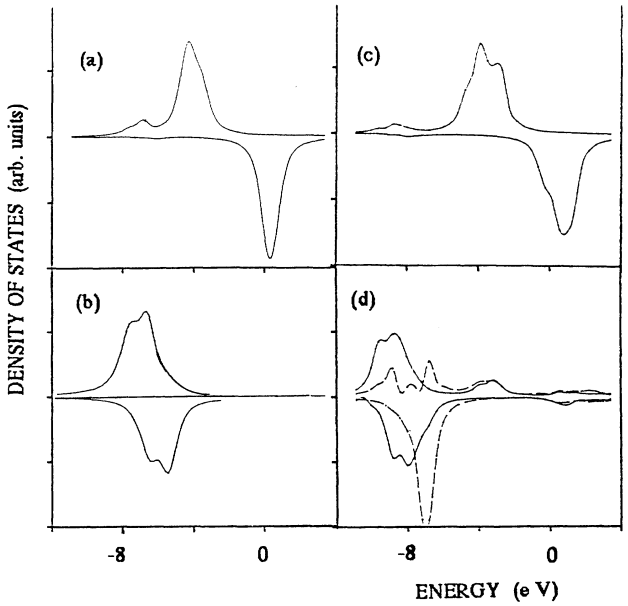

FIG. 4. Partial densities of states in idealized FeO. (a) Fe_4O_4:Fe $3d$; (b) O $2p$; (c) $FeO_6Fe_{12}O_8$: central Fe $3d$; (d) O_6 (——) and O_8 (— — —) $2p$.

eV. However, the set $\{O_6\}$ which is closer to full coordination shows a deeper $2p$ band centered around 8.7 eV. If we accept $\{Fe_1\}$ and $\{O_6\}$ as the best representatives for cations and anions in the system, then we can derive other parameters of relevance in constructing a semiempirical one-electron energy level diagram for FeO, as attempted variously by Eastman and Freeouf,[24] by Balberg and Pinch[25] and by Bagus *et al.* We find the following.

(a) Δ_{CF} $(=10Dq)$ $=0.90$ eV for the initial state Fe^{++} and $=1.20$ eV for the final states, multiplet and crystal-field-split levels of Fe^{+++}. $10Dq$ is the crystal-field splitting of the t_{2g} and e_g one-electron orbitals due to their covalent mixing and electrostatic interaction with the ligands. Although not known experimentally for FeO, $10Dq$ is 1.3 eV for Fe^{++} in aqeous solution; for the final state, Alvarado's analysis of the ESP spectra yields 1.70 ± 0.1 ev for $10Dq$. Thus our calculated values fall short of the experimental results by about 30%. Bagus *et al.* obtain 0.81 eV for the initial state and 1.1 eV for the final states from *ab initio* self-consistent field (SCF) and configuration-interaction wave functions for a $(FeO_6)^{10-}$ cluster simulating FeO, values that are close to what we obtain. It appears then that both HF and the local-density approximation consistently underestimate the relaxation effects that would accurately describe the crystal-field splitting.

(b) $\Delta_{ds}=2.25$ eV is the energy difference from the last occupied d level to the $4s$ band of Fe. From Balberg and Pinch, the optical transition corresponding to Δ_{ds} is associated with the absorption edge measured at 2.0 eV.

(c) $\Delta_{ps}=6.1$ eV is the energy separation between the O $2p$ and the Fe $4s$ bands, commonly estimated at 5.6 eV.

(d) Δ_{ex}, the exchange splitting between spin-up and spin-down orbitals of the same cation, is 4.5 eV.

Considering the obvious limitations of the small ionic basis set in describing the DOS of FeO, we have also carried out control calculations on the embedded 8- and 27-atom clusters using neutral atomic basis for both Fe and O, compacted with the same potential well as for the ionic bases. As expected with neutral bases, large overlap between states centered on neighboring atoms gives sizable occupations for the more diffuse states; also the transfer of charge from Fe to O as measured by volume-integrated charges or by Mulliken population analysis decreases sharply. Thus from the Fe_4O_4 cluster, the orbital occupations for Fe ($3d^{6.17}$, $4s^{0.68}$, $4p^{0.51}$, ionicity equal to $+0.64$, spin equal to $4.30\mu_B$) and O ($2s^{1.94}$, $2p^{4.70}$, ionicity equal to -0.64, spin equal to $0.20\mu_B$) from the 8-atom cluster are more symptomatic of covalent bonding. This is in contrast to the very small value of 0.05 previously estimated for the covalency,[22,23] indicating very little ligand character for the d-shell orbitals.

When the energy distribution curve from the 27-atom cluster is deconvoluted into its contributions from individual atomic orbitals, (see Ref. 24), we see that the main $2p$ peak from the $\{O_6\}$ set is centered around 6.5 eV, the $3d$ spectrum from the central Fe is spread more broadly up to ~7.5 eV below the Fermi level with a peak at 3.8 eV and smaller d-p hybrid structures are located at 1.5 and 3.0 eV. This picture, then, is more consistent with the DOS observed by Grenet *et al.* except for the spillover of O $2p$ to higher energies. The other similarly calculated parameters for this basis set are the following: $\Delta_{CF}=0.88$ eV, $\Delta_{ds}=0.55$ eV, and $\Delta_{ps}=0.55$ eV. Finally, we have a result for the 27-atom cluster embedded using a magnetic unit cell, twice the size of the standard chemical cell, wherein the arrangement of cation spins in adjacent (111) planes is antiparallel. The dominant feature of the cumulative DOS is the complete symmetry in energy between the spin-up and spin-down cation sites.

The cohesive energy of the lattice is a particular property which seems to be insensitive to charge analysis, ionicities, and basis sets chosen. In Table I, we summarize the cohesive energy results for the idealized wustite lattice using several different embedded clusters. For example, the 12- and 16-atom clusters are formed by stacking adjacent pairs of FeO molecules atop each other; the 15-atom clusters are composed of a pair of 8-atom clusters adjoined along the (111) direction and sharing either a Fe or an O atom; adjoining the same along the (110) direction gives the 14-atom cluster. Each of these clusters is a reference cluster in the idealized lattice for a defect structure derived from it. The inequivalent atom sites in these clusters are specified separately to facilitate visualizing the formation of defects by the removal of different sets of cations. These and all further calculations are carried out at the equilibrium lattice constant $a=8.15$ a.u. with the embedding potential from the crystal atoms external to the cluster generated from the self-consistent charges and spins obtained from the 8-atom cluster results, i.e., the "divalent" ions have a net charge of ±1.90 instead of ±2.0; this accounts for the fractional value of the total number of electrons in the noneutral clusters. In this sense we sacrifice full crystal periodicity to gain a more detailed look at the different inequivalent sites in the clusters. This is a legitimate procedure since it (a) eliminates the cruder process of averaging the potential over all sites, (b) fixes the crystal potential from a unit cell at a set value, and (c) most closely parallels the treatment of inequivalencies in the derived defect structures for which they serve as reference ideal lattice calculations.

From Table I, the only recognizable trend in the charge densities, ionicities, and spin found for different cluster sites is that cations closer to the center and anions around the periphery of clusters are slightly more charged, by about $0.10e$. The individual orbital occupation numbers and spins are only very little different from the values obtained from the 8-atom cluster and have not been presented. The Fermi level shows a small dispersion around -2.60 eV; the d-s gap is now spread from 1.87—2.48 eV as orbitals from different cluster atoms of the same kind sample different environments and broaden the energy bands. For the sake of comparison, the cohesive energies quoted are an average over the atoms in the embedded cluster. For the neutral clusters, they increase slightly in the sequence from 8- to 16-atom clusters, from 11.20—11.67 eV, indicating that the extreme atoms on the larger stack clusters do not see the full crystal potential due to the finite size of the microcrystal. The comparatively lower values for the averaged binding energies of the non-neutral 15-atom clusters (10.96 and 10.80 eV) are mostly an indication of the limitations of our eigenvalue-

partitioning scheme as well as a result of the clusters unusual shape. Indeed the only relevant quantity for our future reference is the total cohesive energy of the entire embedded cluster. On the other hand, it is precisely the subtle differences in the reference system that enable us to obtain a consistent picture of the binding in defects.

B. Isolated and simple defects

In the first two rows of Table II, we summarize results from embedded 27-atom cluster calculations of the ground-state energies and charge densities of an isolated cation vacancy and for a ferric cation at a normal octahedral site in FeO. Thus it requires 22.17 eV to remove an Fe^{++} ion from its lattice site to infinity, while the energy cost of replacing a regular octahedral (octa) Fe^{++} by an octahedral Fe^{+++} is 26.43 eV. These values are with reference to free atoms and an ideal lattice, treated quasiperfectly as explained above, i.e., the reference ideal FeO lattice calculation is the 27-atom result from Table I.

In the absence of a ferrous cation, about 0.40 electrons from the $2p$ orbitals of the neighboring $\{O_6\}$ relax into the vacated region raising the Fermi energy to 5.33 eV and pushing O $2p$ higher and closer to the Fermi energy with broadened DOS structures at 6.3 and 3.0 eV. However, the outer $\{O_8\}$ anions relax compensatingly and their $2p$ levels are now centered about 8.5 eV. This indicates the value of a 27-atom cluster in energy calculations in comparison with a highly charged 7-atom cluster $(FeO_6)^{-9.5}$ which in trial runs was found inadequate for calculating energy differences since the characteristic length of interaction in the above defect formation is larger than the size of the cluster. This mechanism—raised Fermi energy and destabilized anions around a cation vacancy—is a signature feature common to all vacancies in the system. Indeed the effect is more pronounced as the number of cluster vacancies adjoining the anion grows. The reverse effect is seen in the presence of an octahedral Fe^{+++}. The extra attraction lowers the Fermi level to -6.36 eV, and pulls the $2p$ levels from the adjacent anions down to about ~ 10 eV. The $3d$ (Fe^{+++}) levels are now around 4.6 eV and the unoccupied Fe $4s$ levels are well above the Fermi level so that the d-s gap is enlarged to 9.6 eV. There is no substantial change in the O $2p$ and Fe $3d$ levels and occupations of the outer atoms.

We shall use the above results for individual defects to study simple aggregates containing vacancies, octahedral Fe^{+++} and tetrahedral cations, as outlined in the remainder of Table II. Since neighboring defects are believed to be at least $2.5a$ apart, it is reasonable to treat each defect structure as isolated in an otherwise perfect lattice. The octahedral Fe^{+++} ions that screen the defect and provide for the neutrality of the microcrystal as per Eq. (17), are not a part of the variational cluster; they are placed at cation sites immediately adjacent to the cluster chosen, as rigid sources of the crystal potential represented via the results of column 2 from Table II so that their contributions to the total energy and net binding energy are exactly known. This procedure is preferable to expanding the variational clusters to include the next shell of ions (e.g., from 8-atom sites to 32-atom site clusters which are the next smallest clusters possible), a procedure that becomes intractable for the larger defects. Chou *et al.*[26] have used such large clusters in a x-ray absorption near-edge spectroscopy (XANES) study of wustite; they find the next shell of atoms to be already very bulklike and self-consistent convergence a tedious process.

The calculated binding energies are quoted with respect to the energies of the component isolated defects and comparison between defects of different shapes and sizes is made possible via the binding energy per net number of vacancies. Thus the aggregate of a cation vacancy with a pair of Fe^{+++} ions is bound by 0.27 eV relative to a lone vacancy while two vacancies when brought together repel each other by 1.43 eV. Since the clusters used for these two calculations are very different, it is not clear whether the two results deserve direct comparison. For the compensated defect, the orbital populations and DOS structures relative to the Fermi energy change very little; the increase in binding comes from the lowering of the Fermi energy (to 0.06 eV) and the one-electron energies. For the 2:0 defect, the oxygens in the cluster adjacent to the two vacancies are left unbound and their dangling bonds are mainly responsible for the overall repulsion. However, introducing a ferric cation at a tetrahedral site bounded by these two vacancies increases the binding to 1.74 eV. The central cation provides a strong bonding center for all four oxygens in the cluster and more than compensates for the decrease in octahedral Fe^{+++} around the cluster from 4 to 1. Interestingly, with a net charge of 2.29 (and net spin 3.87), with its main $3d$ energy levels just 1.0 eV below the Fermi energy and its $4s$ levels located ~ 7.0 eV above the Fermi energy, the tetrahedral cation is clearly a different species from a conventional ferrous or ferric octahedral cation. It is obvious from this trend that the presence of interstitial cations stabilizes the formation of defect structures to a greater degree than any combination of cation vacancies and octahedral Fe^{+++}. This is consistent with the findings of previous semiempirical theories[5,6] and the extensive experimental data from crystallographic[2,3] and electron microscopy studies.[4]

An alternative approach to obtaining an energetically favorable defect structure is to start with a cation jammed into a tetrahedral site of a stoichiometric FeO lattice (a 0:1 defect) and to remove, one-by-one, the nearest-neighbor octahedral cations surrounding the tetrahedral site, as outlined in Table II. In row 5, we see that the presence of a Fe^{+++} ion at such an interstitial site is opposed by an energy barrier of 11.2 eV. To make the calculation more realistic, the distance to the nearest-neighbor cations is relaxed by 0.27 to 3.81 a.u., which is the halfway point between an ion coordinated octahedrally (4.07 a.u.) and one coordinated tetrahedrally (3.53 a.u.) in FeO. Even when the distance is increased to 4.07 a.u., the barrier drops to just 8.7 eV. However, the removal of two of the surrounding octahedral cations (i.e., the 2:1 defect) sharply increases the binding to 1.74 eV, even without relaxing the coordination distance to the other two cations. With the removal of a further octahedral cation, (the 3:1 defect), the binding energy for the defect increases to 3.97 eV. Finally, in the 4:1 defect, with no cations present in the nearest-neighbor sites around the

TABLE II. Simple defects in $Fe_{1-x}O$.

Cluster description	Cluster symmetry	Valence e^- in cluster	No. cluster atoms	No. octahedral Fe^{+++}	Fermi energy (eV)	d-s gap (eV)	Self-consistent ionicities (spins)	Relevant atomic orbital occupations	Energy of formation	Binding energy per net vacancy (eV)
					Cation vacancy system					
$V_1O_6Fe_{12}O_6$	O_h	183.8	26	0	+5.33	+1.68	V −0.39 (0.04) O_6 −1.63 (0.21) Fe_{12} 1.77 (4.29) O_8 −1.86 (0.03)	V 1s 0.13 2p 0.25 O_6 2p 5.64 O_8 2p 5.89	22.17	
					Octahedral Fe^{+++} system					
$Fe_1^{+++}O_6Fe_{12}O_8$	O_h	188.95	27	0	−6.36	2.52	Fe_1 2.85 (4.69) O_6 −1.77 (0.06) Fe_{12} 1.90 (4.12) O_8 −1.92 (0.08)	Fe_1 3d 4.88 (4.43) 4s 0.22 4p 0.05 O_6 2p 5.82 O_8 2p 5.92	−26.43	
					1:0 defect system					
$V_1O_6Fe_{12}O_6$	O_h	183.8	26	2	0.04	1.93	V −0.40 (0.04) O_6 −1.68 (0.18) Fe_{12} 1.80 (4.22) O_8 −1.87 (0.03)	V 1s 0.14 2p 0.26 O_6 2p 5.70 O_8 2p 5.90		−0.27
					2:0 defect system					
$V_2Fe_2O_2O_2$	T_d	43.8	6	4	−0.61	2.96	V_2 −0.27 (0.01) Fe_2 1.68 (4.71) O_2 −1.79 (0.09) O_2 −1.54 (0.14)	O_2 2p 5.81 O_2 2p 5.56		2.85/2 = 1.43
					0:1 defect system					
Fe(t)Fe_4O_4	T_d	61.15	9	0	−11.55		Fe(t) 1.56 (3.02) Fe_4 1.99 (4.22) O_4 −1.64 (0.10)	Fe(t)3d 5.72 (4.27) 4s 0.23 (0.02) 4p 0.23 (0.03) O_2 2p 5.68		+8.42
					2:1 defect system					
Fe(t)$V_2Fe_2O_2O_2$	C_{2v}	48.95	7	1	−8.07	2.43	Fe(t) 2.29 (3.87) V_2 −0.13 (0.01) Fe_2 1.84 (4.01) O_2 −1.72 (0.09) O_2 −1.61 (0.13)	Fe(t)3d 5.55 (3.88) 4s 0.05 4p 0.09 O_2 2p 5.74 O_2 2p 5.64		−1.74/1 = −1.74

TABLE II. (*Continued*).

Cluster description	Cluster symmetry	Valence e^- in cluster	No. cluster atoms	No. octahedral Fe^{+++}	Fermi energy (eV)	*d-s* gap (eV)	Self-consistent ionicities (spins)	Relevant atomic orbital occupations	Energy of formation	Binding energy per net vacancy
					3:1 defect system					
Fe(*t*)Fe_1V_3	C_{3v}	42.85	6	3	−4.85	2.02	Fe(*t*) 2.55 (4.17) Fe_1 1.82 (3.91) V_3 −0.10 (0.01) O_1 −1.58 (0.08) O_3 −1.79 (0.07)	Fe(*t*) 3*d* 5.36 (4.18) 4*s* 0.03 4*p* 0.06 O_1 2*p* 5.60 O_3 2*p* 5.81		−4.02/2 = −2.01
					4:1 defect system					
Fe(*t*)V_4O_4	T_d	36.75	5	5	−2.94	4.10	Fe(*t*) 2.85 (4.57) V_4 −0.08 (0.01) O_4 −1.82 (0.04)	Fe(*t*) 3*d* 5.13 (4.57) 4*s* 0.00 4*p* 0.02 O_4 2*p* 5.84		−8.15/3 = −2.72
					4:1 defect with $Fe^{++}(t)$ system					
Fe(*t*)Fe_4O_4	T_d	37.7	5	6	+6.84	3.86	Fe(*t*) 2.17 (4.30) V_4 −0.12 (0.00) O_4 −1.85 (0.02)	Fe(*t*) 3*d* 5.72 (4.27) 4*s* 0.03 4*p* 0.08 O_4 2*p* 5.89		−5.84/3 = −1.95

tetrahedral Fe^{+++}, the binding energy for the defect cluster is dramatically enhanced to 8.15 or 2.71 eV per net vacancy. Figure 5(a) is a plot of the binding energy of these defects versus the number of valence electrons in the defect cluster. Since the slope of the graph does not level out, one is tempted to search for more complicated defects using the same 9-site cluster format. It is clear that removing further cations from the next shell of ions to form more extended defects would have an effect on the binding energies some order of magnitude less than considered above; this is not a worthwhile avenue to pursue. The answer lies, as we shall see, in placing the ferric cations in adjoining tetrahedral sites so as to minimize their repulsion.

The successive removal of Fe^{++} in the sequence of defect clusters from 0:1 through 2:1 to 3:1 to 4:1 is accompanied by several distinct trends that provide some insight into the increase in cluster binding. The Fermi energy plotted in Fig. 5(b) as a function of the number of electrons in the cluster, rises almost linearly in response to the competition between the growing number of vacancies (m) and the growing number of octahedral ferric cations ($2m-3n$), albeit in the next shell. The charge on the tetrahedral cation increases monotonously from 1.56 to 2.85 for the 4:1 defect; simultaneously the net spin increases from 3.02 to 4.57. Since the $4s$ and $4p$ levels of the central Fe are virtually unoccupied, this is due mainly to the loss of minority spin $3d$ electrons. Other than specifying the total number of electrons in the defect cluster to ensure neutrality for the microcrystal, there are no restrictions imposed on these calculations. Thus the trend towards trivalency ($\sim 3d^5$) of the central cation is a natural outcome of the system's movement towards an energy-minimum configuration. In Figs. 6 and 7, we

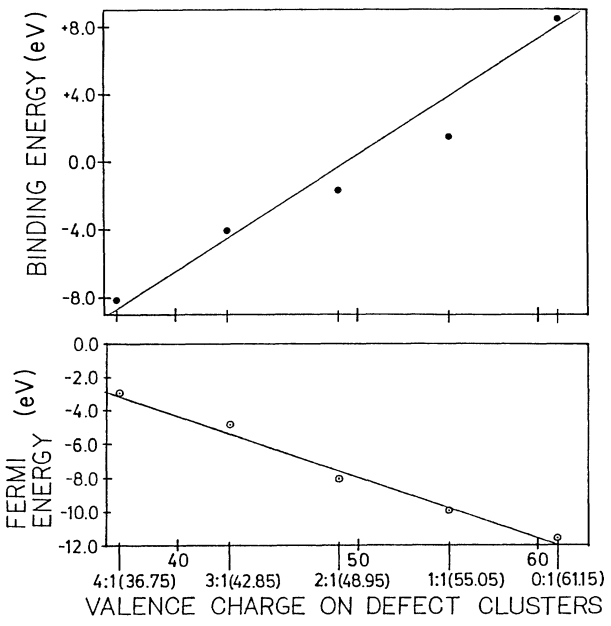

FIG. 5. Variation of properties under stepwise assembly of 4:1 defect cluster: (a) binding energy; (b) Fermi energy.

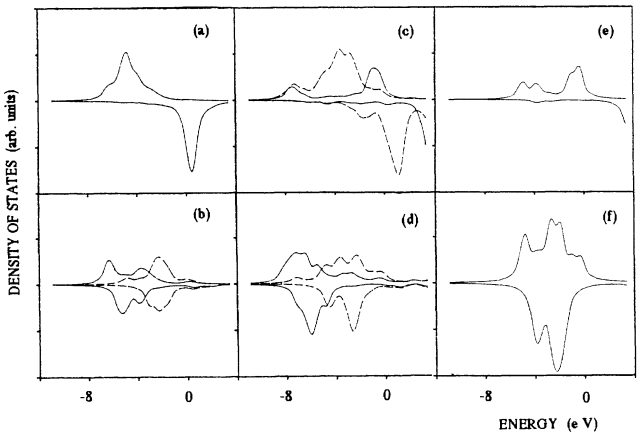

FIG. 6. Comparison of partial densities of states in defect clusters: (a) 2:0 Fe $3d$; (b) O_2^1 $2p$ (——), O_2^2 $2p$ (— — —); (c) 2:1 Fe(t) $3d$ (——), Fe(O) $3d$ (— — —); (d) O_2^1 $2p$ (——), O_2^2 $2p$ (— — —); (e) 4:1 Fe(t) $3d$; (f) O $2p$.

compare the density of states obtained for the 2:0, 2:1, and 4:1 defects. The common features of the DOS for the central cation shows the occupied $3d$ levels just ~ 1.0 eV below the Fermi energy and a smaller d-p hybrid structure around 6—7 eV, which becomes more prominent as the Fe^{++} are removed due to bonding with the octahedral O anions. Thus it is conceivable that a 5 to 10% defect concentration x in a $Fe_{1-x}O$ crystal would manifest itself as the shallow x-ray photoelectron spectra (XPS) peak at 1.5 eV observed by Grenet *et al.*[21] and also contribute to the O $2p$ spectrum near 6.0 eV. The $3d$ levels from the octahedral Fe^{++}, if any, shift progressively higher from 4.0 to 2.6 eV for the 3:1 cluster, its utility as a bonding center being undermined. Further, as the octahedral Fe^{++} are removed, the oxygen anions in the cluster are no longer equivalent and the 9-site cluster exhibits as low a symmetry as C_{3v} and C_{2v}. Typically, as the number of cluster vacancies surrounding anions increases from 1 to 2 to 3, their $2p$ levels broaden and shift towards lower binding, from ~ 7.0 eV through ~ 4.0 to 2.0 eV relative to the Fermi energy. If we had chosen larger clusters to study these defects, specifically by including the next shell of atoms with the octahedral Fe^{+++}, the shifts in the DOS spectrum would not be so exaggerated, the errors due to the nonvariational treatment of the octahedral Fe^{+++} would be partially eliminated and the configuration changes in binding energy would be reduced. However, it is unlikely that such larger clusters would affect the trend of results obtained here.

Another confirmation that the transition to trivalency of the interstitial cation is not a spurious effect is provided by studying a 4:1 defect with a Fe^{++} cation at its center; this is done simply by adding one electron (0.95e to be exact) to the cluster and adjusting the number of octahedral Fe^{+++} around the cluster for neutrality. The binding energy of such a cluster drops to 5.84 or 1.95 eV per net vacancy. It is obvious from the orbital populations that while anions have full $2p$ bands and are stable, the central Fe would rather lose its minority spin charge and tend towards being trivalent. On the other hand, the

removal of one electron from the 4:1 cluster leaves the central cation in its trivalent state ($3d^{5.03}$, ionicity=2.95) and is drawn mainly from the O $2p$ levels (O $2p^{5.61}$, ionicity=-1.59); the result is nonbinding by 3.78 eV. In Fig. 8, the binding energy of the 4:1 cluster is plotted as a continuous function of its valence charge. Points 2 and 4 on the curve, which correspond to an excess or deficit of half an electron around the trivalency point that cannot be neutralized by an integral number of octahedral Fe^{+++} ions, are obtained by simulating the absence and/or presence of the half-electron by a uniform neutralizing charge spread over the surface of a sphere of a radius 6.5 a.u. Certainly, the 4:1 defect with a Fe^{+++} cation is closest to the minimum point on the curve. It is safe to conclude from these results that the 4:1 (Fe^{+++}) defect would dominate over other simple defect structures in wustite.

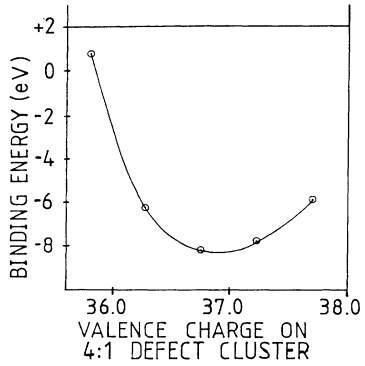

FIG. 8. Binding energy of the 4:1 defect as a function of the cluster valence charge.

At this stage, it is instructive to analyze the sources of systematic and random errors to check the limits of reliability of our results. Self-consistency is pursued until the Fermi energy and the eigenvalues are converged to within 0.001 eV; the discrepancy between parametrized input and output potential vectors is considerably less than 0.001. Using the 0:1 and 4:1 clusters as representatives, we find that the binding energy is converged to within 0.02 eV with regards to the Gauss-quadrature grid and to within 0.50 eV with respect to the diophantine mesh in the interstitial region. These values are simply obtained by doubling the density of points in the G-q grid and tripling the sampling density of the diophantine scheme separately, the errors being expectedly larger for the 0:1 cluster. Replacing the Mulliken analysis by a least-squares fit to the charge density reduces the divalent ionicities by about 0.20 but otherwise leaves the major trends of results unaffected. Extending the basis to include further virtual orbitals for both Fe and O is known to enhance the binding; however, its effect is overwhelmed by the integration errors for the sampling densities we presently use. The frozen-core approximation overestimates the core shift contribution to the cohesive energy by 0.42 eV for the Fe_4O_4 cluster and by proportionately less as Fe^{++} ions are removed. This leaves us with two critical model limitations discussed below. In reality, when the distribution of octahedral Fe^{+++} around a given defect cluster is not symmetric, it disturbs the equivalency of cluster atomic sites for which the potential and charge densities are averaged so that it is not always possible to find the configuration that minimizes the energy. This is especially true for the aggregates of the 4:1 defect for which the possible placement permutations are larger. The essential criteria followed in arranging these Fe^{+++} ions are the following: (a) simple symmetry of arrangement, (b) preferred proximity to center of clusters, and (c) preferred filling of sites with highest number of nearest-neighbor vacancies. In this sense the lattice binding energy results presented here are not exhaustive since all possible configurations for a m:n defect have not been tested. We estimate from limited experimentation [see comments on the 7:2 (110) cluster below] that the spread in binding energies due to this would not exceed ± 0.20 eV per net vacancy. An alternate scheme, wherein the charge neutralizing the defect cluster is now spread over the surface of a sphere of radius equal

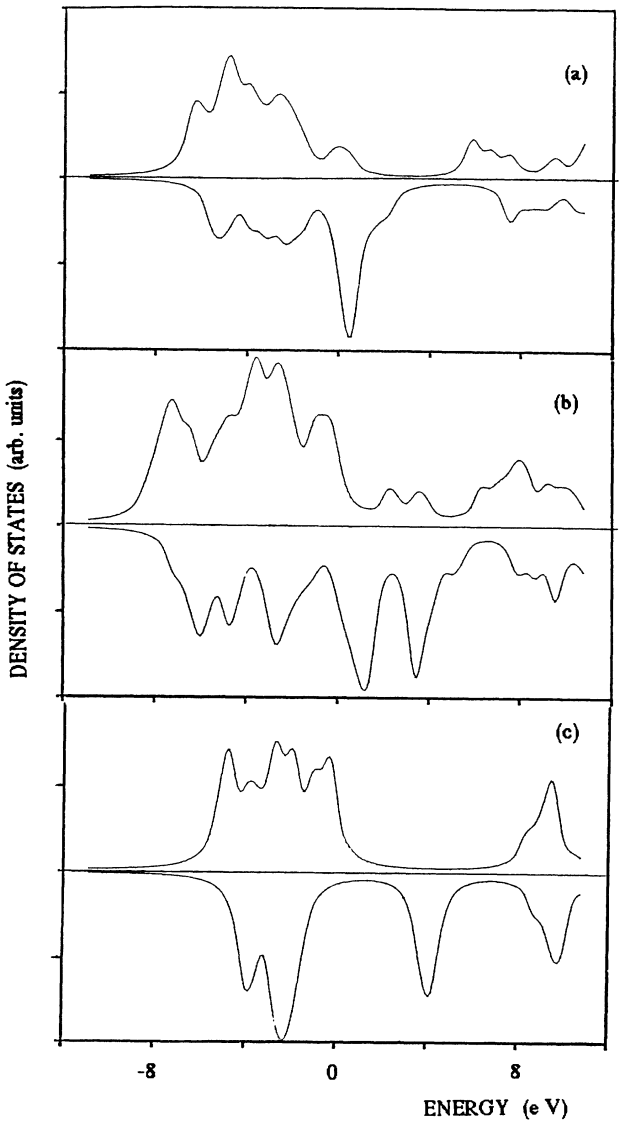

FIG. 7. Comparison of total densities of states in defect clusters: (a) 2:0; (b) 2:1; (c) 4:1.

to the average distance of the Fe^{+++} octahedral ions from the center of the cluster (which is 6.5 a.u. for the 9-site cluster format), although unrealistic, yields reliable binding energies and is used in instances where the number of required octahedral Fe^{+++} is negative (e.g., 0:1 and 1:1 defects) or fractional. The second major limitation is the small size of the "minimal" clusters which precludes any relaxation effects in the shell of the octahedral Fe^{+++} in the crystal.

C. Larger clusters

We now turn our attention to aggregates of the basic 4:1 defect. The only two ways by which this defect can grow in size are by edge sharing of vacancies (e.g., 6:2 and 8:3 defects) or by corner-sharing of vacancies (7:2, 8:2, and 13:4 defects studied here). The clusters used to study these defects have been diagrammed in Fig. 9. The treatment of these defect clusters is identical to that used for the ones treated above, the results are displayed in Table III and compared with previous calculations of the lattice defect internal binding energies by Catlow and Fender[5] and by Anderson and co-workers.[6] By stacking 4:1 defects atop each other, the additional tetrahedral bonding centers lower the Fermi energy from -2.94 eV (4:1) to -5.77 eV (8:3). This is an expected repeat of what we found in going from the 2:0 to the 2:1 defect and contrasts with the rise in Fermi energy as the number of octahedral vacancies around a tetrahedral cation increases. The *d-s* gap for the tetrahedral Fe^{+++} is again sharply widened to 8.4 eV. The charge on the centermost Fe^{+++} in the 8:3 cluster is now just 2.27; i.e., it is squeezed into regaining some of the minority spin $3d$ charge and tends to behave rather like a divalent cation; its $3d$ levels peak at 2.0 eV (which is between ~ 4.0 eV for Fe^{++} and ~ 1.0 eV for Fe^{+++}) with smaller structures at 4.75 eV, 6.0 eV, and 7.7 eV due to bonding with the $2p$ levels from the surrounding O atoms. The effect is less noticeable on the outer ferric cations which behave more conventionally like those found at the center of the 4:1 cluster. The $2p$ levels from the O atoms follow the same trends in the presence of cluster vacancies discovered previously with an added dimension: the inner oxygen are more strongly bound to the central Fe^{+++} (DOS at 6.0 eV) than to the outer two Fe^{+++} (DOS at ~ 2.3 eV). The overall effect is that the binding energy per net vacancy decreases monotonously from 2.72 eV (4:1) to 1.23 eV (8:3); note that the net binding for the 6:2 defect exceeds that for the 4:1 defect by 1.26 eV. Thus edge sharing of 4:1 clusters does not appear to be energetically favorable.

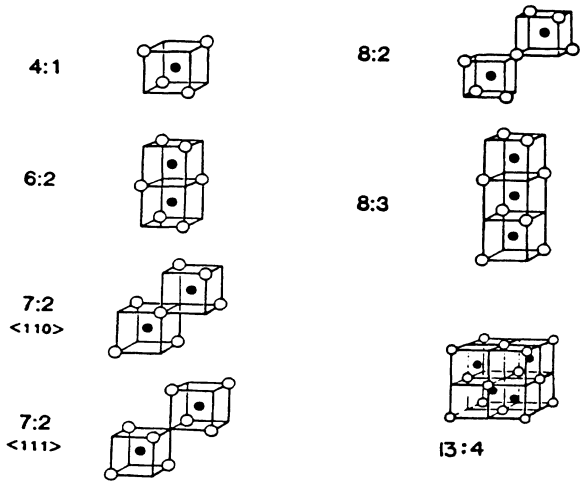

FIG. 9. Pictorial representation of some aggregates of the 4:1 defect.

The repulsion between the tetrahedral cations can be reduced and minimized by adjoining the 4:1 clusters along the (110) and (111) directions which yields the pair of 7:2 defects and the 8:2 defect. Of these three, it is the 7:2 (110) defect which exhibits the largest binding, 3.94 eV per vacancy. Indeed all of them are considerably more stable than the component 4:1 defects by between 0.5 and 1.22 eV per net vacancy.

For the 4:1 and its aggregate defects, we also carried out self-consistent calculations with the cluster bond lengths expanded to 4.40 a.u. from 4.07 a.u., an 8% increase commensurate with the relaxations in lattice positions suggested by Koch and Cohen and Cheetham *et al.* When compared with results for the unrelaxed lattice, we find very little change in the orbital occupation numbers and spin populations (less than 0.05 change in ionic charge) and in the DOS structure relative to the Fermi level. The Fermi energy itself drops in proportion to the number of bond lengths changed for all clusters by about 0.08—0.12 a.u. and the *d-s* gap for the tetrahedral Fe^{+++} is narrowed by about 0.50 eV. The binding energy increases in every case without disturbing any trends found for the unrelaxed clusters. The smaller increases in binding for the 7:2 defects are due to only the cluster sites being relaxed while nearby sites in the crystal in the same shall of atoms are left unchanged. Further, there is evidence to show that the next shell of atoms relaxes inwardly;[28] with so many coordinate variables finding an optimum Fe^{+++}—O^{--} bond length is not a practical pursuit.

Koch and Cohen[2] (KC) obtained the best fit to their x-ray diffraction data by using a relaxed 13:4 cluster. Our self-consistent calculation of the KC cluster, with just the cluster atom positions relaxed by 8%, shows a rather small binding energy per net vacancy of just 1.1 eV. This defect cluster then is apparently not a serious contender as a favorable configuration and its popular use may be put under question.

IV. CONCLUDING DISCUSSION

There is widespread acceptance both from diffraction data and from microscopy studies[1-4,28-30] that vacancy clusters dominate in $Fe_{1-x}O$; the dominant cluster and the functional dependence of the related vacancy-to-interstitial ratio r with temperature and concentration x are still subject to debate. The most ordered phase of wustite P'',[4] exhibits a cubic superstructure of clusters whose separation is $2.5a$ in two planes and are offset by $0.5a$ in the third direction. Lattice imaging techniques in

TABLE III. Aggregates of 4:1 defect in $Fe_{1-x}O$.

Cluster description	Cluster symmetry	Valence electrons in cluster	No. cluster atoms	No. octahedral Fe^{+++}	Fermi energy (eV)	Self-consistent ionicities (and spins)	Binding energy per net vacancy (eV)	Binding energy per net vacancy (eV) (relaxed clusters)	Ref. 6	Ref. 5
						4:1 defect system				
$Fe(t)V_4O_4$	T_d	36.75	5	5	−2.94	$Fe(t)$ 2.85 (4.57) V_4 −0.08 (0.01) O_4 −1.82 (0.04)	−8.15/3 = −2.72	−11.58/3 = −3.86	−0.62	−1.98
						6:2 defect system				
$Fe_2(t)V_2V_4O_2O_4$	D_{2h}	57.7	7	6	−4.87	$Fe_2(t)$ 2.72 (4.54) V_2 −0.15 (0.03) V_4 −0.12 (0.00) O_2 −1.66 (0.06) O_4 −1.76 (0.10)	−9.41/4 = −2.35	−14.01/4 = −3.50	−0.69	−2.42
						8:3 defect system				
$Fe_1(t)Fe_2(t)V_4V_4O_4O_4$	D_{2d}	78.65	11	7	−5.77	$Fe_1(t)$ 2.27 (4.20) $Fe_1(t)$ 2.67 (4.29) V_4(in) −0.06 (0.04) V_4(out) −0.15 (0.01) O_4(in) −1.69 (0.05) O_4(out) −1.66 (0.06)	−6.14/5 = −1.23	−10.23/5 = −2.05	−0.72	−2.52
						7:2 (110) defect system				
$Fe_2(t)V_1O_1V_4V_4V_2O_2$	C_{2v}	65.6	9	8	−2.24 −3.52	$Fe_2(t)$ 2.81 (4.60) O_1 −1.41 (0.05) V_4 −0.16 (0.01) O_4 −1.81 (−0.01) V_2 −0.14 (0.01) O_2 −1.73 (0.08)	−19.70/5 = −3.94	−20.10/5 = −4.02	−0.65	
						7:2 (111) defect system				
$Fe_2(t)V_1V_6O_2O_6$	C_{2v}	73.6	10	8	−4.43	$Fe_2(t)$ 2.79 (4.69) V_1 −0.14 (0.04) V_6 −0.13 (0.01) O_2 −1.83 (0.02) O_6 −1.57 (−0.03)	−17.98/5 = −3.60	−18.4/5 = −3.68	−0.75	

TABLE III. (*Continued*).

Cluster description	Cluster symmetry	Valence electrons in cluster	No. cluster atoms	No. octahedral Fe^{+++}	Fermi energy (eV)	Self-consistent ionicities (and spins)	Binding energy per net vacancy (eV)	Binding energy per net vacancy (eV) (relaxed clusters)	Ref. 6	Ref. 5
					8:2 (111) defect system					
$Fe_2(t)O_1O_6V_2V_6$	C_{3v}	65.6	9	10	+0.56	$Fe_2(t)$ 2.83 (4.70)	−19.45/6= −3.24		−0.47	
						O_1 −1.24 (0.06)				
						O_6 −1.83 (0.03)				
						V_2 −0.12 (0.01)				
						V_6 −0.13 (0.01)				
					13:4 (Koch-Cohen) system					
$Fe_4(t)V_1O_6V_{12}O_8$	C_{2v}	131.2	18	14	+0.55	$Fe_4(t)$ 2.71 (4.69)		−9.90/9= −1.10	−0.40	−2.10
						V_1 −0.15 (0.03)				
						O_6 −1.68 (0.15)				
						V_{12} −0.14 (0.01)				
						O_8 −1.76 (0.07)				

electron microscopy[28] have narrowed the estimate of the number of vacancies per cluster to around 5. Any number of stable condensates of the 4:1 defect, formed via edge- or corner-sharing and commensurate with P'' are conceivable. However, only those with $m:n$ ratios between 2 and 4 are known to form; in this phase a $m:n$ ratio would correspond to a defect concentration of $x=(m-n)/4(2.5)^3$.[29] It is clear from the experimental literature[30] that r is not at present a useful quantity in determining the dominant cluster(s) in wustite; the allowed values of r, given the experimental uncertainty, span the range of predicted values based upon the multitude of clusters proposed. Besides, it is also conceivable that long-range ordering under some conditions can call for a number of distinct cluster types to coexist in equilibrium.

Calculations of defect processes using static lattice methods within various approximations have long existed and accurate values for the defect formation enthalpies, activation energies, cluster binding energies, and so on, have been obtained for many systems. A fine recent review of these methods is provided by Catlow and Mackrodt.[31] Since experimental measurements are carried out at constant pressure and usually at high temperatures, it is more practical to augment internal energy calculations, such as ours, with methods to calculate the equally important entropies of formation and migration of defects, of which there are now three adequate methods in the literature.[32] The estimate of the free energy of defect formation[33,34] could then be used to adjudicate the choice of clusters as parameter fits to the x-ray diffraction data, and a host of measured quantities, e.g., conductivity, thermopower, Seebeck coefficients, Mössbauer spectra,[35] etc. In view of the previous comments, it is not the purpose of the present study to exhaust the manifold of possible representative defect clusters; although the technology is manifestly present, it would serve little purpose. Presently, though, while the accuracy of the values of the lattice energies calculated here are unknown, the relative energies and trends do form the basis for interpretation. We thus restrict ourselves to elucidating the energetics that emerge.

Considering the absolute minimal basis employed on the anions, we have modeled a nearly inert anion sublattice, with little ability to relax electronically; one must not be misled by the extreme jumps in the DOS structures from the O $2p$ orbitals, a definite cluster size effect. The primary electronic delocalizations are provided by the ionic orbitals on the Fe species, both octahedral and tetrahedral; even then very little charge is seen to relax into the vacancies. It appears therefore that it is the ionic nature of the basis set chosen that allows a reasonable picture of the interaction energies in defect clusters to emerge in spite of the very reduced number of valence orbitals. As it is, the differences in binding energy of the defect clusters obtained in our work are much larger than the previous theoretical results[5,6,27] on similar defects as seen from Table III.

Comparison of a 1:1 and a 2:1 defect indicates that the Fermi energy increase of 1.90 eV in the latter case reduces the contribution from the sum of one-electron eigenvalues

towards the binding energy by approximately 6.3 eV. This energy gain, along with the electrostatic repulsion due to two extra octahedral Fe^{+++} is more than overcome by the reduction in the electrostatic opposition to a Fe^{+++} at a tetrahedral site; the net result is that the 2:1 defect is more stable by 3.24 eV. In going from a 2:0 to a 2:1 defect, both the Fermi energy and the one-electron eigenvalue sum are depressed towards greater binding energies, by 7.46 and ~ 15.7 eV, respectively. They thereby assist with the reduction in electrostatic repulsion due to three fewer octahedral Fe^{+++} and the presence of an additional tetrahedral Fe species; the net result is that the 2:1 defect is better bound by 4.59 eV. This is a major difference between the defect stabilization afforded by the octahedral and tetrahedral Fe^{+++} ions and raises the interesting possibility of bringing octahedral Fe^{+++} ions "closer to the action," i.e., placing them in the same shell as the Fe^{++} that are ejected. This is precisely what happens in the condensates of the 4:1 defect in which efficient use of vacancies and Fe^{+++} leads to considerably increased binding energies. For the 7:2 and 8:2 clusters, some of the octahedral Fe^{+++} reside in the same nearest-neighbor shell as the residual vacancy holes; the energy lowering due to their attractive potential outweighs the repulsion between the interstitial ions. Such a proximal arrangement is not possible for the 6:2, 8:3, and 13:4 clusters; the octahedral Fe^{+++} are at least one shell removed and despite the attempt of the tetrahedral Fe to relax to "mixed ferro-ferric" status, the cluster binding energy per vacancy decreases with increasing size. In this scenario clusters made up of adjoining incomplete tetrahedra have a viable chance of being energetically competitive only with judiciously placed proximal octahedral Fe^{+++}. This is not a utilitarian conclusion since it opens up an entire class of possible defect clusters not derived as conglomerates of the 4:1 defect. Even the unexpected stability ordering of the 7:2 and 8:2 clusters may with a little thought be partly understood in terms of this broad criterion.

We carried out three tests on the 7:2 (110) defect with the 8 octahedral Fe^{+++} in different sites (actually from simple symmetry considerations only 3 of the 8 Fe^{+++} need to be shifted around). Our results for the binding energy varied from 3.89—4.11 eV per net vacancy, a spread which represents the highest end of the influence of approximations to our results, and is still less than the difference between defect binding energies to be compared. Thus the 7:2 (110) defect does exceed the 7:2 (111) defect in stability. The 4:1 clusters with a Fe^{+++} and a Fe^{++} at their center differ only on two counts: the 0.95 additional electronic charge and the extra octahedral Fe^{+++} for the latter cluster. Part of this difference in binding for these two cases is the result of changing from one incomplete basis set to another for the central Fe.

In summary, self-consistent calculations of the internal lattice defect energies of prototypical defect clusters in nonstoichiometric $Fe_{1-x}O$ are presented using the embedded cluster approximation within the Hartree-Fock-Slater $X\alpha$ formalism. The energetics show that a tetrahedral "ferric" species in the interstitial site stabilizes a defect structure to a greater degree than any combination of vacancies and octahedral Fe^{+3}. Definite trends in the valence DOS, the Fermi energy and the cluster binding energies indicate that the 4:1 cluster dominates over all other simple combinational clusters with a single tetrahedral Fe^{+3}. Of the larger aggregates of the 4:1 defect studied, the 7:2 (110) cluster exhibits maximum stability. An analysis of the individual contributions to the formation energy reveals that the proximity of the average charge-compensating configuration of octahedral Fe^{+3} around the defect cluster is a fair indicator of the relative stability of a defect. Lastly, the XPS structure near the Fermi energy is shown to come from the $3d$ levels of Fe^{+3} in the tetrahedral sites.

ACKNOWLEDGMENTS

The work of D.E.E. was supported by the U.S. Department of Energy, Grant No. DE-FG02-84ER45097. M.R.P. acknowledges support through the Northwestern University Materials Research Center, under National Science Foundation (NSF) Grant No. DMR-82-16972.

[1]W. L. Roth, Acta Crystallogr. **13**, 140 (1960).
[2]F. Koch and J. B. Cohen, Acta Crystallogr. B **25**, 275 (1969).
[3]A. K. Cheetham, B. E. F. Fender, and R. I. Taylor, J. Phys. C **4**, 2160 (1971).
[4]C. Lebreton and L. W. Hobbs, Radiat. Eff. **74**, 227 (1983).
[5]C. R. A. Catlow and B. E. F. Fender, J. Phys. C **8**, 3267 (1975); C. R. A. Catlow, B. Fender, and D. G. Muxworthy, J. Phys. (Paris) Colloq. **38**, C7-67 (1977).
[6]A. B. Anderson, R. W. Grimes, and A. Heuer, J. Solid State Chem. **55**, 353 (1984).
[7]J. C. Slater, *The Self-Consistent Field for Molecules and Solids* (McGraw-Hill, New York, 1974).
[8]B. Delley, D. E. Ellis, A. J. Freeman, E. J. Baerends, and D. Post, Phys. Rev. B **27**, 2132 (1983).
[9]C. X. Guo and D. E. Ellis, Phys. Rev. B **31**, 5006 (1985).
[10]D. E. Ellis, G. A. Benesh, and E. Byrom, Phys. Rev. B **16**, 3308 (1977); B. Lindgren and D. E. Ellis, *ibid.* **26**, 636 (1982).
[11]E. J. Baerends, D. E. Ellis, and P. Ros, Chem. Phys. **2**, 41 (1973); D. E. Ellis and G. S. Painter, Phys. Rev. B **2**, 2887 (1970).
[12]M. Tinkham, *Group Theory and Quantum Mechanics* (McGraw-Hill, New York, 1964).
[13]C. B. Haselgrove, Math. Comp. **15**, 323 (1961); D. E. Ellis, Int. J. Quantum Chem. **2S**, 35 (1968).
[14]A. H. Stroud, *Approximate Calculation of Numerical Integrals* (Prentice-Hall, New Jersey, 1971), p. 296.
[15]*Handbook of Mathematical Functions,* edited by M. Abramovitz and I. A. Stegun (Dover, New York, 1972), p. 916; K. Fukushima, J. Mizuno, K. Fujima, and H. Adachi, J. Phys. Soc. Jpn. **51**, 4028 (1982).
[16]R. S. Mulliken, J. Chem. Phys. **23**, 1833 (1955); **23**, 1841 (1955); B. Delley and D. E. Ellis, *ibid.* **76**, 1949 (1982).

[17]M. P. Tosi, in *Solid State Physics,* edited by F. Seitz and D. Turnbull (Academic, New York, 1964), Vol. 16, p. 1.
[18]V. L. Moruzzi, J. F. Janak, and A. R. Williams, *Calculated Electronic Properties of Metals* (Pergamon, New York, 1978).
[19]R. W. G. Wyckoff, *Crystal Structures,* 2nd ed. (Interscience, New York, 1963), Vol. 1.
[20]T. C. Waddington, Adv. Inorg. Chem. Radiochem. **1**, 157 (1959).
[21]G. Grenet, Y. Jugnet, T. M. Duc, and M. Kibler, J. Chem. Phys. **72**, 218 (1980).
[22]P. S. Bagus, C. R. Brundle, T. J. Chuang, and K. Wandelt, Phys. Rev. Lett. **39**, 1229 (1977).
[23]S. F. Alvarado, M. Erbudak, and P. Munz, Phys. Rev. B **14**, 2740 (1976).
[24]D. E. Eastman and J. L. Freeouf, Phys. Rev. Lett. **34**, 395 (1975).
[25]I. Balberg and H. L. Pinch, J. Magn. Magn. Mater. **7**, 12 (1978).
[26]S. H. Chou, J. Guo, and D. E. Ellis, Phys. Rev. B **34**, 12 (1986).
[27]C. R. A. Catlow and A. M. Stoneham, J. Am. Ceram. Soc. **64**, 234 (1981).
[28]S. Ijima, Proceedings of the International Conference on Real Atoms and Real Crystals, Melbourne, Australia, 1974, p. 135.
[29]J. R. Gavarri, C. Carel, and D. Weigel, J. Solid State Chem. **29**, 81 (1979).
[30]E. Gartstein and T. O. Mason, J. Am. Ceram. Soc. **65**, C24 (1982); E. Gartstein, J. B. Cohen, and T. O. Mason (private communication).
[31]C. R. A. Catlow and W. C. Mackrodt, in *Computer Simulations of Solids,* Vol. 166 of *Lecture Notes in Physics,* edited by C. R. A. Catlow and W. C. Mackrodt (Springer, New York, 1982), Chap. 1.
[32]J. H. Harding and A. M. Stoneham, Philos. Mag. B **43**, 705 (1981); P. W. M. Jacobs, M. A. Nerenberg, and J. Govindrajan, *Computer Simulations of Solids,* Vol. 166 of *Lecture Notes in Physics,* edited by C. R. A. Catlow and W. C. Mackrodt (Springer, New York, 1982), Chap. 2; J. H. Harding, Physica **131B**, 13 (1985). In order, the references describe a supercell technique, a Green's-function method and a SHEOL (simple harmonic evaluation of lattices) code calculation of the lattice entropy.
[33]A. M. Stoneham, S. M. Tomlinson, C. R. A. Catlow, and J. H. Harding, *Physics of Disordered Materials,* edited by D. Adler, H. Fritzsche, and S. R. Ovshinsky (Plenum, New York, 1985), p. 245.
[34]R. Tetot and C. Gerdanian, J. Phys. Chem. Solids **46**, 869 (1985).
[35]N. N. Greenwood and A. T. Howe, J. Chem. Soc. (Dalton Trans.) **1**, 110 (1972); **1**, 116 (1972); **1**, 122 (1972).